Research Article

Zhong Xu*, JiaNing Wu, Min Zhao, ZhiJie Bai, KunYun Wang, JieWei Miao, and ZhuoYue Tan

Mechanical and microscopic properties of fiber-reinforced coal gangue-based geopolymer concrete

https://doi.org/10.1515/ntrev-2022-0033
received December 10, 2021; accepted January 3, 2022

Abstract: In order to explore the engineering application potential of coal gangue-based geopolymer concrete (CGGPC), this article formulated the fiber-reinforced coal gangue-based geopolymer concrete (FRCGGPC). The mechanical properties of the specimens were tested to analyze the effects of different types and dosing amounts of fibers on the mechanical properties of CGGPC. The microscopic morphology of the specimens was observed by scanning electron microscopy (SEM) to analyze the strengthening mechanism of fibers on the mechanical properties of the CGGPC. The experimental results show that the splitting tensile strength of FRCGGPC can be improved obviously, but the improvement of compressive strength is not obvious. The control groups containing steel fiber (SF) and polyester fiber (PF) had peaks in their compressive strength. Under the same dosage, the effect of SF and PF on the splitting tensile strength of FRCGGPC is better than basalt fiber. The results of SEM analysis show that within a certain range of dosage, the fiber is closely combined with the matrix, which has a good force transmission effect and strengthens the matrix material. When the fiber dosage is too much, it is easy to agglomerate, which leads to the decrease in the mechanical properties of the specimens.

Keywords: geopolymer concrete, coal gangue, fiber-reinforced concrete, mechanical properties, microscopic morphology

1 Introduction

Geopolymer is a new type of green engineering material developed in recent years, first discovered and named by French scientist Prof. Joseph Davidovits in 1970s [1–3], which is formed by inorganic aluminosilicate natural minerals or solid wastes as raw materials under alkaline exciter conditions by appropriate process. Since the concept of geopolymer was proposed, scholars have been greatly interested. A large number of studies have shown that geopolymer materials have excellent mechanical properties and durability [4–6], a wide range of raw materials, simple processes, low production energy consumption, and low pollution. It is an environmentally friendly green building material, which can be widely used in construction engineering [7], traffic engineering [8], *etc*. At present, research on geopolymer concrete (GPC) is still relatively scattered, and the engineering application is also limited due to the lack of systematic theoretical support and sufficient experimental data [9–15]. Therefore, the targeted comprehensive performance test and mechanism analysis of GPC are the key works and research points that need to be carried out urgently at this stage.

At present, among the many experimental explorations of GPC, scholars more often use fly ash (FA) [16,17], slag [18–20], and metakaolin [21,22] as cementitious material to prepare new GPC in order to improve the mechanical properties and durability of GPC. However, for coal gangue (CG) as an important geopolymer raw material, relatively few researchers carry out mechanical properties test, and carry out inadequate mechanistic analysis [23–25]. As one of the industrial wastes with the largest emissions all over the world, CG is mainly composed of aluminosilicate minerals and carbon, rich in silica and alumina and abundant in reserves. It can also be used to prepare GPC by mixing with other silica-alumina raw materials to optimize strongly. The mechanical properties of GPC can be complemented

* **Corresponding author: Zhong Xu,** College of Environment and Civil Engineering, Chengdu University of Technology, Chengdu 610059, China, e-mail: xuzhong@cdut.edu.cn
JiaNing Wu, Min Zhao, ZhiJie Bai, KunYun Wang, JieWei Miao, ZhuoYue Tan: College of Environment and Civil Engineering, Chengdu University of Technology, Chengdu 610059, China

by the characteristics of different materials. Geng *et al.* used low-calcium red mud and physically excited kaolinite CG as raw materials to prepare dual-doped geopolymers. The experimental results proved that the strength of the geopolymer synthesized by mechanical grinding and preactivation was relatively higher [26]. Huang *et al.* mixed calcined CG, granulated slag, and lime to prepare geopolymer [27]. The experiment proved that the low dosage of active calcium in CG was the reason for the low strength of geopolymer. The increase in the granulated slag and lime would increase the dosage of active calcium and the strength. Zhang *et al.* proved through experiments that destroying the stable kaolinite structure and improving the activity of CG is one of the effective methods to change the reactivity of CG. By this way, CGGPC can improve its comprehensive mechanical properties [24]. The above studies show that it is feasible to prepare CGGPC meeting the performance requirements by mixing CG with other silica-alumina raw materials under the premise of ensuring the activity of CG. Further exploration of engineering performance is the basis for the popularization and application of CGGPC.

In the exploration of the engineering performance of GPC, low strength and brittle failure characteristics are the biggest problems faced currently. Many scholars have carried out tentative explorations to solve the problem [28–32]. Saranya *et al.* found that steel fiber (SF) enhances the engineering and durability properties of ground granulated blast-furnace slag-Dolomite GPC and explained how to improve the bond strength and impact resistance by adding SF [33]. Sahin *et al.* analyzed the influence of different proportions of basalt fiber (BF) on metakaolin-based GPC mortar produced with different aggregate types. The results show that BF had a positive effect, especially with the best performance when 0.8–1.2% is used [34]. Research by Gao *et al.* showed that polyester fiber (PF)-reinforced polymer composites as lateral confining materials can improve the strength and ductility of the recycled aggregate concrete significantly [35]. The above studies show that it is of great value to explore the mechanical properties of the CGGPC by adding fibers. The fiber-reinforced CGGPC (FRCGGPC) reflects the idea of composite design, which not only retains the original characteristics of high compressive strength of concrete, but also greatly increases its crack resistance, toughness, and impermeability, making it more in line with the requirements of new construction materials. The magnitude of the effect of fiber concrete on concrete modification depends on the interaction between the fiber and concrete boundary as well as the type, size, density, and direction of fiber distribution in the concrete, which are all related to the microstructure of FRCGGPC. By comparing the mechanical property strengthening effects of incorporating different fibers on CGGPC and exploring their differences in microstructure, we can provide a reference for further selective or composite applications of engineering fiber materials.

Based on the above, this article uses calcined CG as the base raw material and BF, SF, and PF as the reinforcing materials to prepare FRCGGPC. The mechanical properties test and microstructure analysis were carried out, and the effects of different types and dosages of fibers on the mechanical properties of the GPC specimens were compared, and combined with scanning electron microscopy (SEM) its mechanical strengthening mechanism was analyzed. The purpose is to explore the engineering performance and application potential of the CGGPC, and to provide research cases and data support for the development and promotion of the CGGPC.

2 Materials and methods

2.1 Experimental materials

Cementitious materials: calcined CG, low-calcium FA, and blast-furnace slag were all produced by Chuanxing Mineral Powder Factory, Lingshou County, Hebei Province. The physical photographs are shown in Figure 1; the chemical composition analyses are shown in Table 1.

Fiber: BF, SF, and PF were from Changzhou Bochao Engineering Materials Co., Ltd. The physical photographs are shown in Figure 2; the chemical composition analyses of BF, SF, and PF are shown in Tables 2–4, respectively.

Double solution alkali exciter: water glass and sodium hydroxide (NaOH) solution composition.

Fine aggregate: natural river sand, fineness modulus of 2.6–3.0 and apparent density of 2,635 kg/m^3.

Coarse aggregate: continuous graded pebbles, with a particle size of 5–16 mm, an apparent density of 2,745 kg/m^3, a bulk density of 1,460 kg/m^3, and a mud dosage of 0.1%.

Water: ordinary tap water in Chengdu, which meets the relevant technical requirements of “Water Standard for Concrete Mixing” (JGJ63-89).

2.2 Experiment apparatus

The main experiment apparatus used in this test are shown in Table 5.

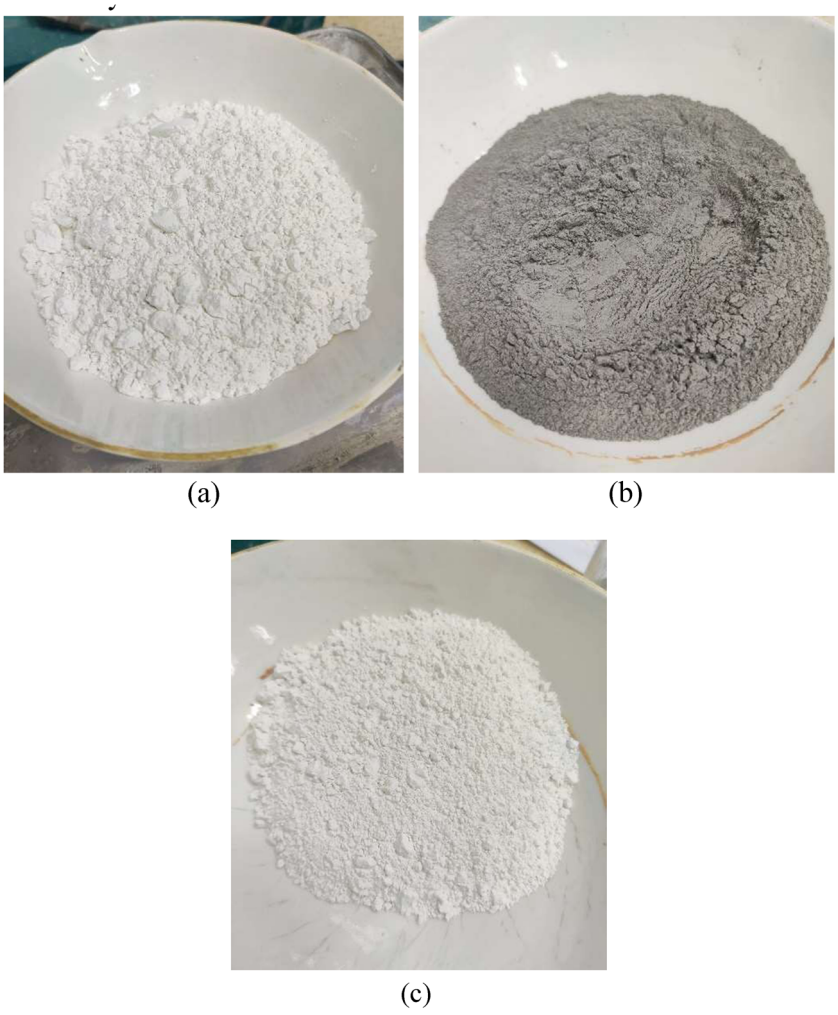

Figure 1: Cementitious materials. (a) CG, (b) FA, and (c) slag.

Table 1: Chemical composition of cementitious materials

Materials	Unit	CG	FA	Slag
SiO_2	wt%	53	65.6	39.2
Al_2O_3		42	8.7	17.6
Fe_2O_3		≤0.5	3.9	—
H_2O		≤0.3	0.01	—
S		0.24	—	—
CaO		—	3.5	36.55
MgO		—	—	4.6
MnO		—	—	1.7

2.3 Casting of specimens

2.3.1 Mix proportion design

The preliminary mix proportion design of materials in this test were based on "Specification for mix design of ordinary concrete" (JGJ 55-2011), "Technical code for the application of mineral admixture" (GB/T 51003-2014), and the existing studies [36].

The mass proportion of calcined CG, low-calcium FA, and blast-furnace slag were determined to be 2:1:1. The mass proportion of water glass to NaOH solution in alkali activator solution was 7:3. The sol proportion was set to 0.5. The mass proportion of solid to water in NaOH solution was about 1:1. After many trials, the optimum proportion of CGGPC material in this test was obtained. In each square meter of CGGPC, the amount of each component of the geopolymer cementitious material was about 247.71 kg calcined CG, 123.85 kg low-calcium FA, 123.85 kg blast-furnace slag, 74.34 kg NaOH solution, 173.47 kg water glass solution, and 13.36 kg sodium hydroxide solid was needed to reduce the modulus of water glass.

The fiber dosage as a variable in this experiment was determined mainly through previous studies [37–39] and

Figure 2: Fibers. (a) BF, (b) SF, and (c) PF.

trial matching. Among the three selected fibers, BF dosage was 0.1, 0.3, and 0.5% of the total volume of FRCGGPC; SF dosage was 0.3, 0.5, and 0.75% of the total volume of FRCGGPC; PF dosage was 0.5, 1.0, and 1.5% of the total volume of FRCGGPC.

The specific mix proportion is shown in Table 6.

2.3.2 Mixing and curing of specimens

Prepare the alkali stimulant 12 h in advance, and let it stand at room temperature for later use. First, the silica-alumina powder material and coarse and fine aggregates were put into the agitator for drying, stirring for 3 min until mixed evenly. Meantime, according to the mix proportion standard, the required fiber was weighed and evenly separated under dry conditions, stirring at low speed for about 3–5 min. Then, the fibers were pulled out from the soaking container and put evenly into the slurry after absorbing the excess water on the surface. Finally, after mixing for 1 min, the concrete mixture was put into the corresponding mold of 100 mm × 100 mm × 100 mm and vibrated to dense.

After the specimens were formed, the surface was covered with impermeable film immediately and placed in an environment with a temperature of 20 ± 5°C for 24 h and then demolded. Subsequently, the specimen was densely wrapped with film membrane, and maintained

Table 2: Performance parameters of BF

Performance	Diameter (μm)	Density (g/cm^3)	Breaking tenacity (MPa)	Modulus of elasticity (MPa)
Parameter	15.0	1.6	1.29×10^3	6.52×10^4

Table 3: Performance parameters of SF

Performance	Length (mm)	Diameter (μm)	Density (g/cm³)	Tensile property (MPa)
Parameter	12	28	5.34	577

Table 4: Performance parameters of PF

Performance	Length (mm)	Diameter (μm)	Density (g/cm³)	Breaking tenacity (MPa)	Initial modulus (MPa)
Parameter	32	28	1.15	864	3.2×10^3

in an oven at 105°C for 12 h. After removal from the oven, it was transferred to a drying room with a temperature of about 20°C for maintenance to a specified age (3, 7, or 28 days), as shown in Figure 3.

According to the design mix proportion, 150 effective cube specimens were finally poured for mechanical performance test and microscopic morphology analysis.

2.4 Strength test

According to "Standard Test Method for Physical and Mechanical Properties of Concrete" (GBT50081-2019), the precast concrete cured to the specified age was taken out and subjected to cubic compressive strength test by using the microcomputer-controlled pressure test machine (WHY-2000) with the measurement accuracy of ±1%, as shown in Figure 4(a). Then, the cubic splitting tensile test was conducted with the assistance of splitting tensile jig and pressure transfer tool to ensure the stability of the specimen during testing, as shown in Figure 4(b). Three specimens were tested in each group, and the average value was taken as the final value. Since the concrete specimens in this test are 100 mm × 100 mm × 100 mm non-standard specimens, the compressive strength and the splitting tensile strength are calculated according to the following formulas (1) and (2), respectively.

$$f_{cu} = 0.95 \times \frac{F}{A}, \tag{1}$$

where F is the compressive failure load, and A is the bearing area of the specimen.

$$f_{ts} = 0.85 \times \frac{2F}{\Pi A} = 0.85 \times 0.637 \times \frac{F}{A}, \tag{2}$$

where F is the splitting failure load, and A is the splitting bearing area of the specimen.

Table 5: Laboratory apparatus

Name	Model
Classifier	Inside diameter: 5–20 mm
Electronic scale	YP3002N
Concrete mixer	—
Specimen mold box	100 mm × 100 mm × 100 mm
Concrete vibration table	ZD/LX-PTP
Electric drying oven	841Y-0
Microcomputer-controlled stress testing machine	WHY-2000
Fixture for splitting tensile test	PLJJ
SEM	S-3000N

2.5 Micromorphology analysis

After the compressive test and splitting tensile test, the residual bulk specimens containing fibers were selected as test specimens, which were divided into 10–20 mm diameter chips. Then, the group with the most obvious strength change in the control group of different mixed CGGPC under the mechanical performance test was selected, and observed by SEM (Thermo Fisher Scientific's Prisma-E), as shown in Figure 5. The microscopic morphology of the matrix after failure was restored to the maximum extent, and the mechanism of the mechanical property test results was analyzed.

3 Research results and discussion

3.1 The influence of different fiber types and dosages on the compressive strength of FRCGGPC

3.1.1 Failure morphology

Figures 6 and 7 show the failure morphology of the specimens in the cube compressive test.

Table 6: Mixed proportion of FRCGGPC (kg/m^3)

Test group	CG	FA	NaOH		Water glass	Water			Sand	Coarse aggregate	Fiber dosage (vol%)
			Preparation of solution	Reduced modulus		Water dosage of sodium silicate	NaOH	External water mode			
CGGPC-0	247.71	123.85	37.17	13.36	173.47	112.76	37.17	57.72	559.67	1039.39	0
BFCGGPC-0.1	247.71	123.85	37.17	13.36	173.47	112.76	37.17	57.72	559.67	1039.39	0.1
BFCGGPC-0.3											0.3
BFCGGPC-0.5											0.5
SFCGGPC-0.3	247.71	123.85	37.17	13.36	173.47	112.76	37.17	57.72	559.67	1039.39	0.3
SFCGGPC-0.5											0.5
SFCGGPC-0.75											0.75
PFCGGPC-0.5	247.71	123.85	37.17	13.36	173.47	112.76	37.17	57.72	559.67	1039.39	0.5
PFCGGPC-1.0											1.0
PFCGGPC-1.5											1.5

Note: CGGPC – coal gangue-based geopolymer concrete; BFCGGPC – basalt fiber-reinforced coal gangue-based geopolymer concrete; SFCGGPC – steel fiber-reinforced coal gangue-based geopolymer concrete; PFCGGPC – polyester fiber-reinforced coal gangue-based geopolymer concrete. The number in the specimen name column indicates the volume of fiber admixture accounted for the proportion of the total volume of FRCGGPC, for example in BFCGGPC-0.1, said BF admixture is 0.1% of the experimental group.

Figure 3: Concrete specimens placed in oven for curing.

Among them, Figure 6 reflects the failure morphology of the benchmark group of specimens after the compressive test. During the test process, this group of specimens has continued to develop cracks, which were large in number and width. Figure 6(a) reflects the situation in the loading process. Subject to the increased compression, the cracks in the middle of the specimens were quickly penetrated, and the surface of the FRCGGPC was gradually spalling off; Figure 6(b) reflects the situation after the end of loading. The skin around the specimen was peeling off seriously, the residual matrix was curved, and the internal aggregate and cement paste were completely exposed. Figure 7 reflects the failure morphology of the control group mixed with different fibers after loading. Although the difference between the failure morphology of CGGPC with different fibers was not obvious, the specimens all showed a certain degree of lateral expansion, and a small number of long cracks occurred on the four side surfaces, accompanied by a small amount of debris falling. The integrity was stronger than the benchmark group, and there was no large-area peeling of the case.

3.1.2 Experimental data and results analysis

As shown in Table 7, the cube compressive strength of the specimens with three different fibers and dosages under standard curing for 3, 7, and 28 day are obtained. Figure 8 shows the law of compressive strength with different fibers and dosages.

It can be seen from Figure 8 that the compressive strength of CGGPC was slightly improved when the

(a) (b)

Figure 4: Strength test laboratory apparatus. (a) Microcomputer-controlled stress testing machine and (b) splitting tensile jig.

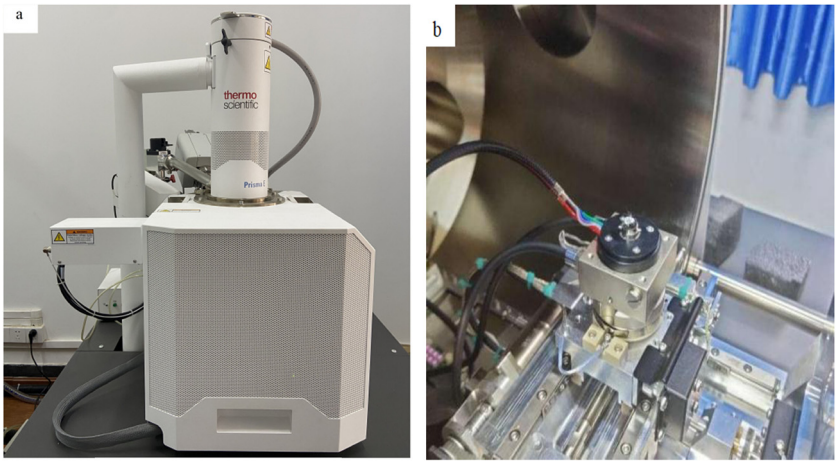

Figure 5: SEM. (a) Instrument appearance. (b) Carrier table.

dosage of three different types of fiber exceeds a certain volume, but it is not significant. When the BF dosage was 0.1, 0.3 and 0.5%, the compressive strength of FRCGGPC reached the maximum of 23.66 MPa (3 days), 25.18 MPa (7 days), and 30.22 MPa (28 days), respectively, which were 7.79, 11.34, and 5.69% higher than those of the benchmark group. When the SF dosage was 0.3%, the compressive strength of FRCGGPC reached the maximum of 23.75 MPa (3 days), 24.04 MPa (7 days), and 30.21 MPa (28 days), respectively, which were 8.22, 6.3, and 6.35% higher than those of the benchmark group. When the PF dosage was 0.5%, the compressive strength of FRCGGPC reached the maximum of 23.94 MPa (3 days), 24.89 MPa (7 days), and 29.93 MPa (28 days), respectively, which were 9.09, 10.08, and 5.35% higher than those of the benchmark group.

It is worth noting that when adding the control group containing SF and PF, the compressive strength of FRCGGPC showed a peak value. Finally, its compressive strength was lower than that of the benchmark group, and the maximum reduction was 12.55%. As shown in Figure 8(b), the compressive strength of the control group reached the peak value when the SF dosage was 0.3%, and then gradually decreased with the increase in the SF dosage. When the SF dosage reached 0.75%, the compressive strength of the control group at 3, 7, and 28 days were all lower than that of the

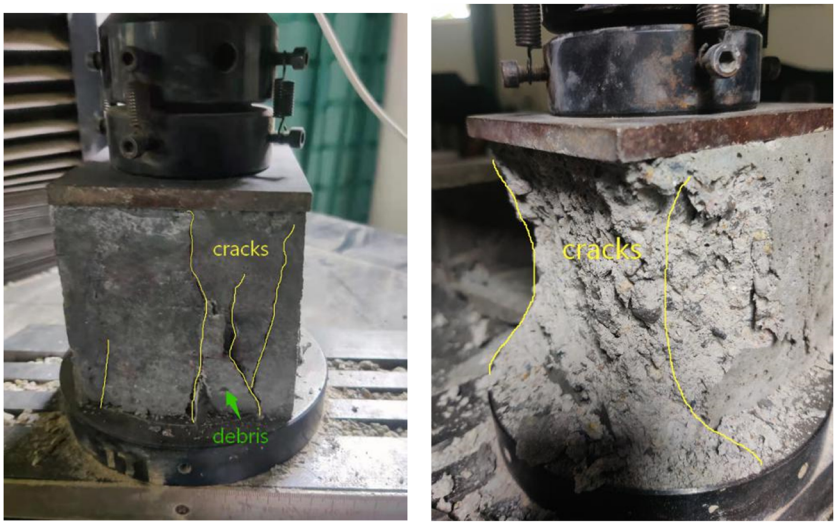

Figure 6: Benchmark group. (a) During fracturing and (b) complete fracturing.

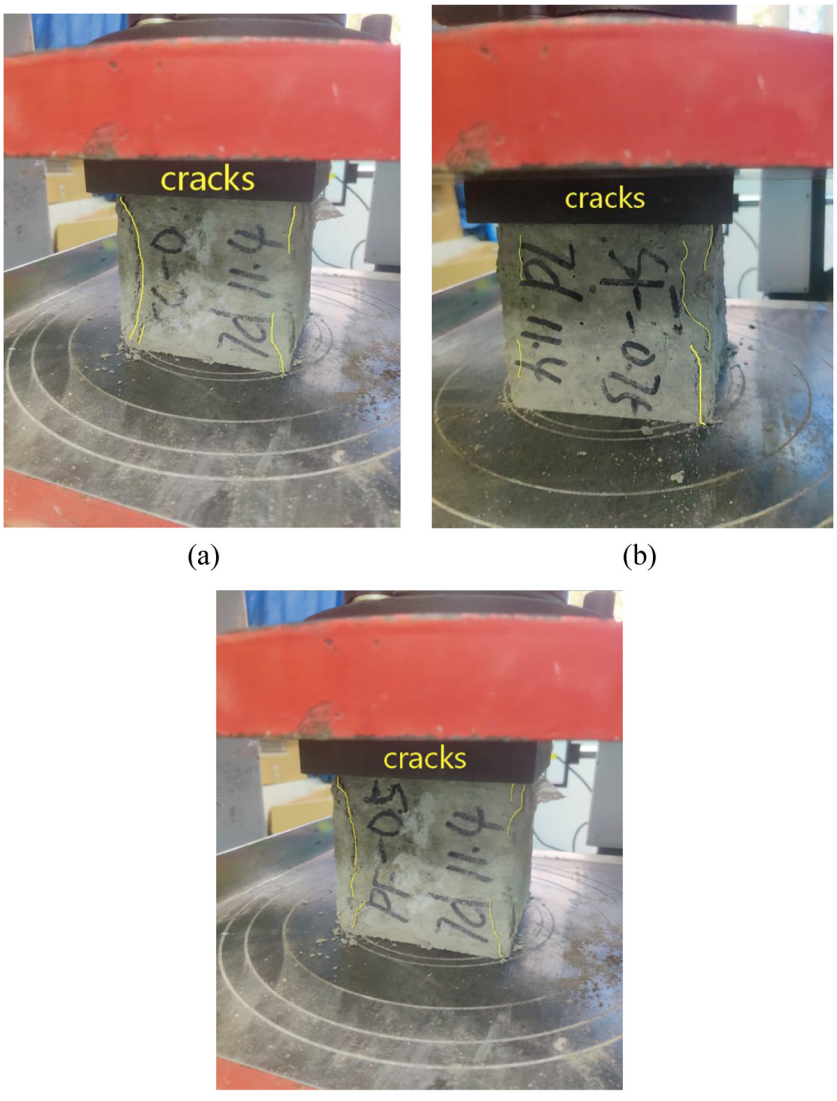

Figure 7: Control groups. (a) BFCGGPC, (b) SFCGGPC, and (c) PFCGGPC.

Table 7: Test results of cube compressive strength

Fiber type	Fiber dosage (vol%)	Serial number	Compressive strength		
			3 days	7 days	28 days
—	0	CGGPC	21.95	22.61	28.41
BF	0.1	BFCGGPC-0.1	22.52	23.85	29.07
	0.3	BFCGGPC-0.3	23.66	24.80	29.83
	0.5	BFCGGPC-0.5	23.56	25.18	30.22
SF	0.3	SFCGGPC-0.3	23.75	24.04	30.21
	0.5	SFCGGPC-0.5	22.14	23.47	28.79
	0.75	SFCGGPC-0.75	19.19	20.71	26.70
PF	0.5	PFCGGPC-0.5	23.94	24.89	29.93
	1.0	PFCGGPC-1.0	21.76	22.04	27.36
	1.5	PFCGGPC-1.5	19.48	19.86	25.56

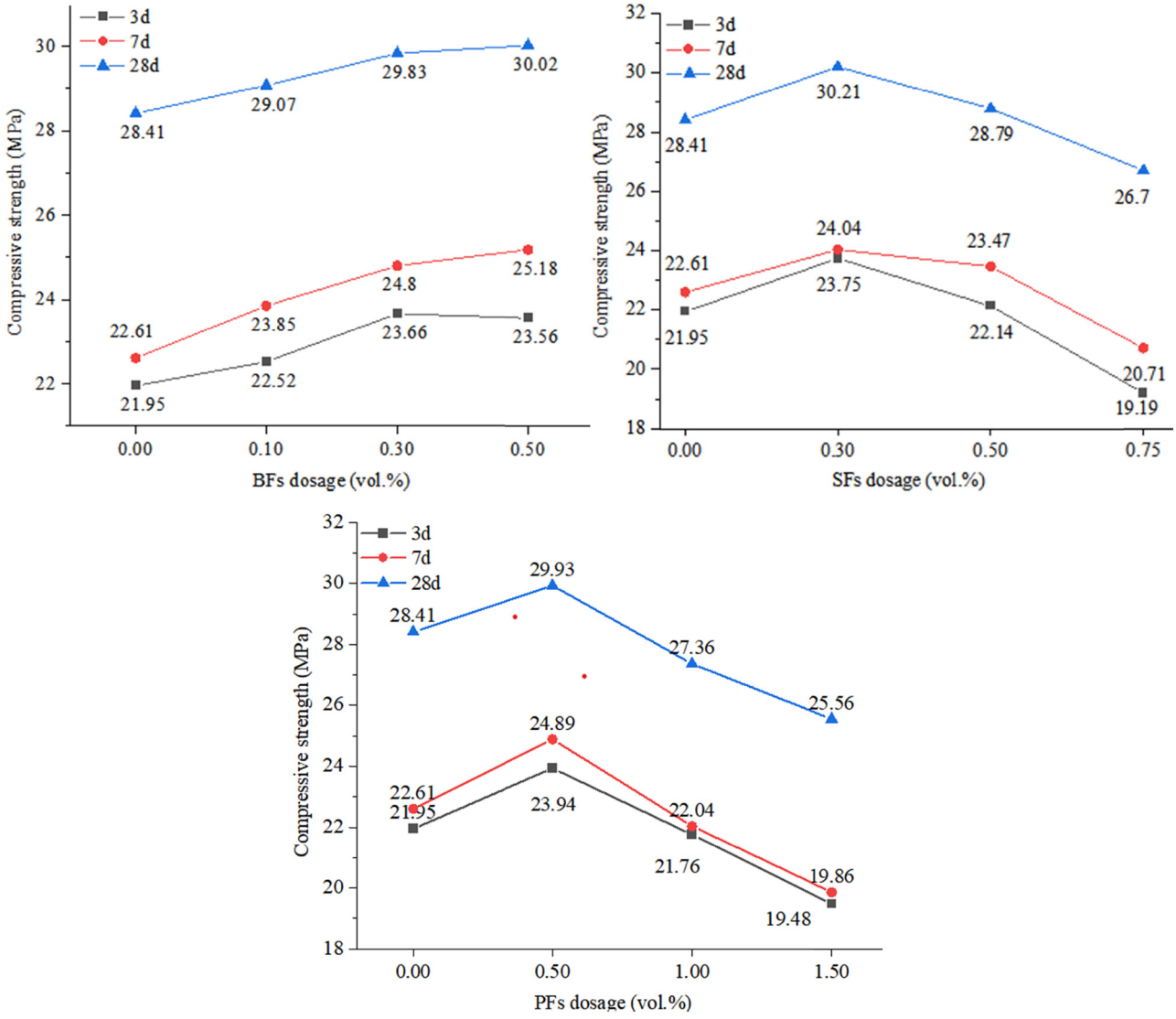

Figure 8: Compressive strength of FRCGGPC.

benchmark group. As shown in Figure 8(c), the change trend of compressive strength of the control group containing PF was similar to that of the SF control group. It can be seen that each fiber has a suitable range of admixtures, and within this range, the compressive strength of FRCGGPC can be slightly improved. However, exceeding its scope will have a certain negative impact on it.

Researchers have confirmed through numerous tests that too much fibers are detrimental to the compressive properties of geopolymer composites [40–45]. One of the reasons is that when the fiber dosage reaches the most suitable proportion, excessive incorporation of fiber will destroy the best structure of the GPC that has been formed. The fiber cannot be wrapped by sufficient slurry, and the specific surface area increases greatly, resulting in the decrease in the density of GPC, the increase in internal defects, and the occurrence of microcracks and pores. The other reason is that the physical form of fibers also affects the compressive strength of FRCGGPC to some extent. The results show that PF and SF are more prone to agglomeration than BF. The agglomerations are aggravated by increasing the amount of dosage, which results in more pores in the mix and less internal continuity, and thus lowering compressive load capacity.

3.1.3 Micromorphology analysis

Figure 9, respectively, shows the 28 days microscopic morphology of benchmark group, the control group BFCGGPC-0.5 group, SFCGGPC-0.5 group, and PFCGGPC-1.0 group under the compressive test.

It can be seen from Figure 9 that the amount of polymerized gel on the surface of the matrix was not affected after the fiber was incorporated, and a few cracks, holes, and unreacted FA particles can be observed on the surface of the matrix. The cracks may be generated by the expansion of high temperature curing, and the holes may be caused by the residual air during mixing and evaporation of mixing water in the matrix after hardening. The incorporation of fibers did not change the properties of the cementitious materials and aggregates subjected to compressive load in the matrix. Therefore, the effect of fiber incorporation on the compressive strength of CGGPC is not obvious.

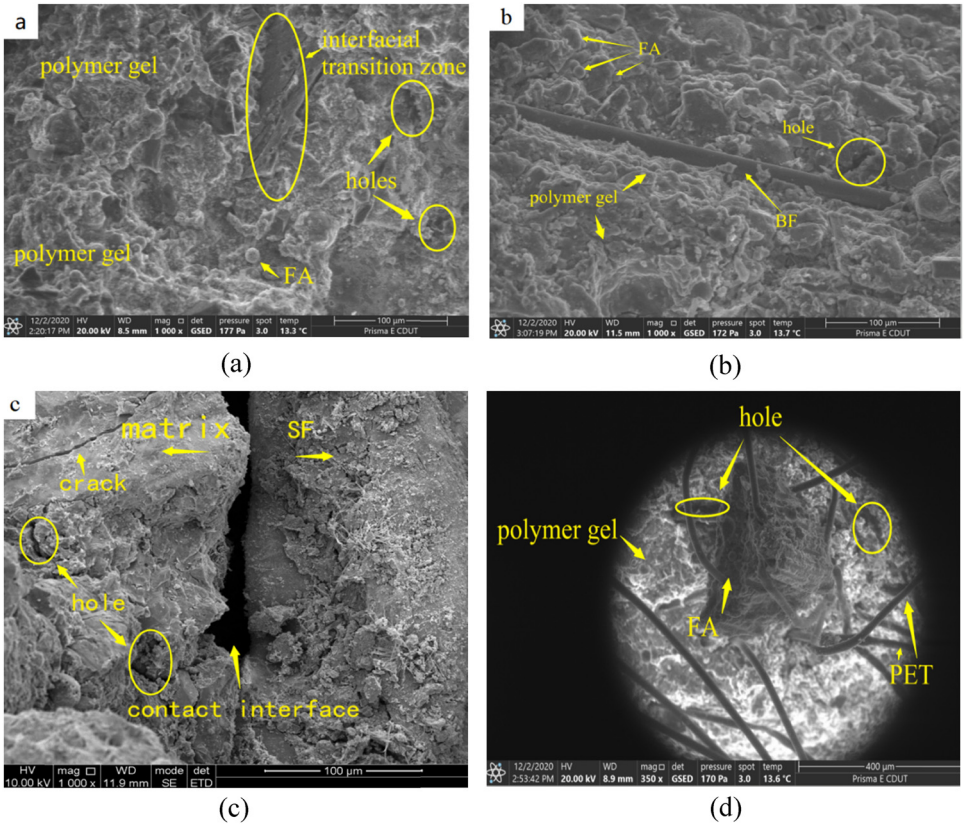

Figure 9: Micromorphology of the matrix after curing for 28 days. (a) CGGPC, (b) BFCGGPC-0.5, (c) SFCGGPC-0.5, and (d) PFCGGPC-1.0.

Based on the analysis from the perspective of microstructure, as shown in Figure 9(b), there was no obvious hole or loose matrix around the BF, and the exposed fiber ends were tightly connected with the geopolymer matrix. There was no significant difference between the overall morphology and the benchmark group. It can be seen that the incorporation of BF has no adverse effect on the matrix. Based on the analysis from chemical composition level, BF as an inorganic fiber, the chemical composition is very similar to that of silica-alumina raw materials. Under the action of alkali activator, Si and Al provided by BF were released and reacted with Na^+ and Ca^{2+} in the environment to generate C–S–H and N/C–A–S–H silicate aluminates, and the polymer gels in the matrix further increased. It can be used as a kind of micro-aggregate in the geopolymer matrix, which helps to improve the compactness and homogeneity of the matrix. Therefore, the compressive strength of the control group containing BF is generally improved [46].

Compared with the other two fibers with smaller diameters, the gap between the SF and the matrix was wider, and the looseness near the matrix was also higher, as shown in Figure 9(c). It is confirmed that the abovementioned SF dosage is too high, causing the porosity in the matrix and the number of interfacial weak areas to increase. Obviously, as shown in Figure 9(d), the PFs agglomerate in this area. There were multiple PFs interwoven in a small field of vision, which were bound to increase the formation of small holes and reduce the coherence between the cementitious materials in the matrix, causing the compressive strength of FRCGGPC to decrease.

3.2 The influence of different fiber types and dosages on the splitting tensile strength of FRCGGPC

3.2.1 Failure morphology

Figures 10 and 11 show the failure morphology of the specimens in the cube splitting tensile test.

Among them, Figure 10 reflects the failure morphology of the benchmark group of specimens after the splitting tensile test. The specimen of this group was not only split in the vertical direction, but also has transverse fracture at the waist. Figure 11 shows the failure morphology of the control group. A small amount of cracks gradually developed from the compression part and finally penetrated, but there was no transverse splitting. The cracked part also appeared in the situation of fiber bridging matrix, which effectively prevented the expansion of cracks. Compared with the benchmark group, the specimens obviously changed from brittle failure to ductile failure. Meanwhile, there were obvious differences in the failure interface of CGGPC with different fibers. The broken interface of BF was difficult to identify the residual fiber, and the interface debris was less, and there was no scattered granular debris distribution. The broken interface of SF has no excessive debris remaining. The broken interface of PF has more debris and a lot of adhesion.

3.2.2 Experimental data and results analysis

As shown in Table 8, the cube splitting tensile strength of the specimens with three different fibers and dosages

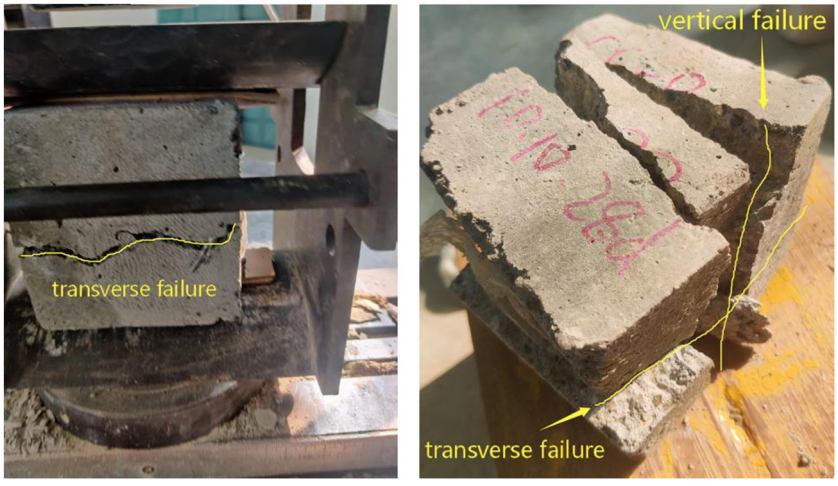

(a) (b)

Figure 10: Benchmark group. (a) During fracturing and (b) complete fracturing.

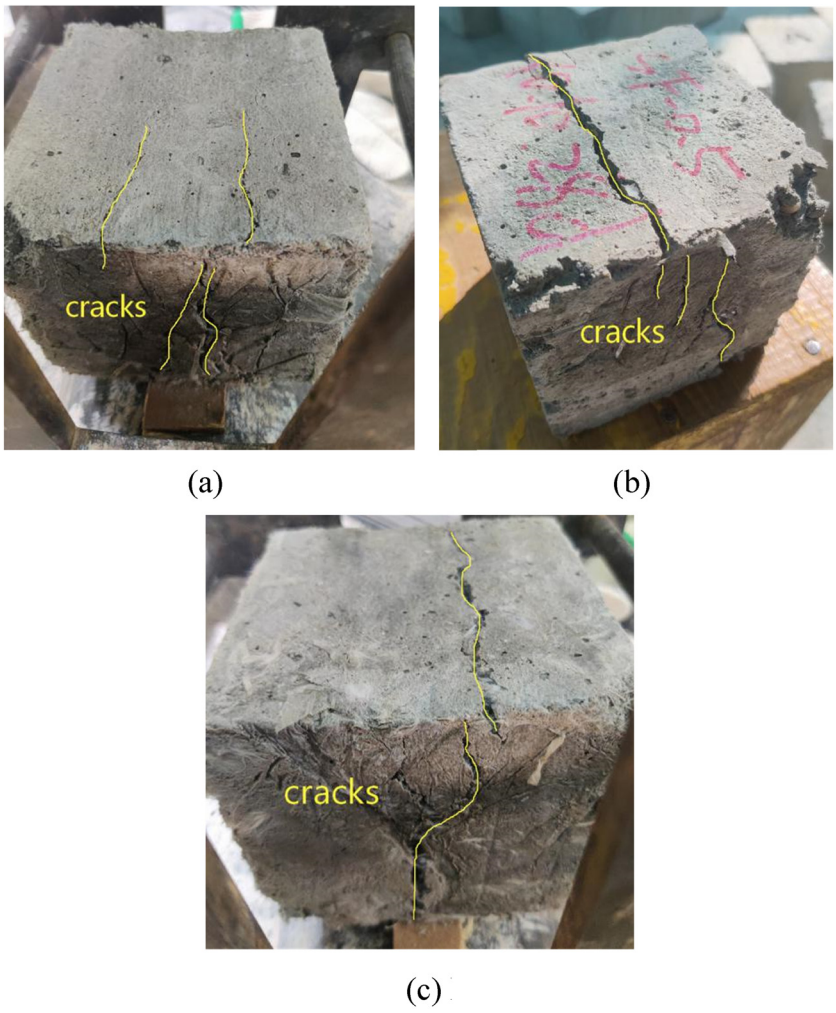

Figure 11: Control groups. (a) BFCGGPC, (b) SFCGGPC, and (c) PFCGGPC.

under standard curing for 7 and 28 days are obtained. Figure 12 shows the law of splitting tensile strength with different fibers and dosages.

It can be seen from Figure 12 that the incorporation of three different fibers has a significant effect on the splitting tensile strength of FRCGGPC. When the BF dosage was 0.5%, the splitting tensile strength of FRCGGPC reached the maximum of 2.16 MPa (7 days) and 2.3 MPa (28 days), which were 51.33 and 46.15% higher than those of the benchmark group, respectively. When the SF dosage was 0.5%, the splitting tensile strength of FRCGGPC reached the maximum of 2.42 MPa (7 days) and 2.62 MPa (28 days), which were 69.64 and 66.80% higher than those of the benchmark group, respectively. When the PF dosage was 1.0%, the splitting tensile strength of FRCGGPC reached the maximum 2.46 MPa (7 days) and 2.73 MPa (28 days), which were 72.32 and 73.68% higher than those of the benchmark group, respectively.

Fiber has a relatively large influence on the splitting tensile strength of FRCGGPC, mainly due to two reasons. First, the fibers act as a restraint to effectively mitigate the lateral deformation of the GPC matrix in the process of being pulled. When the load is further increased resulting in the formation of cracks in the matrix, the crack development in the fiber is restricted, and the crack path is forced to be blocked or transferred. Second, the fiber enhances the bite force between the aggregate and slurry phase materials. The materials of each phase will form a hole when the force is applied, effectively inhibiting the extension of cracks. Although all three fibers can enhance the compressive strength of CGGPC to varying degrees, the fibers can only share a small portion of the transverse tensile stress in the matrix. The strength of FRCGGPC depends on the strength of the aggregate, as well as the interaction between the aggregate and the cementitious material.

Table 8: Test results of cube splitting tensile strength

Fiber type	Fiber dosage (vol%)	Serial number	Compressive strength	
			7 days	28 days
—	0	CGGPC	1.43	1.57
BF	0.1	BFCGGPC-0.1	1.74	2.06
	0.3	BFCGGPC-0.3	1.66	1.95
	0.5	BFCGGPC-0.5	2.16	2.30
SF	0.3	SFCGGPC-0.3	2.22	2.30
	0.5	SFCGGPC-0.5	2.42	2.62
	0.75	SFCGGPC-0.75	2.18	2.54
PF	0.5	PFCGGPC-0.5	2.10	2.58
	1.0	PFCGGPC-1.0	2.46	2.73
	1.5	PFCGGPC-1.5	1.88	2.35

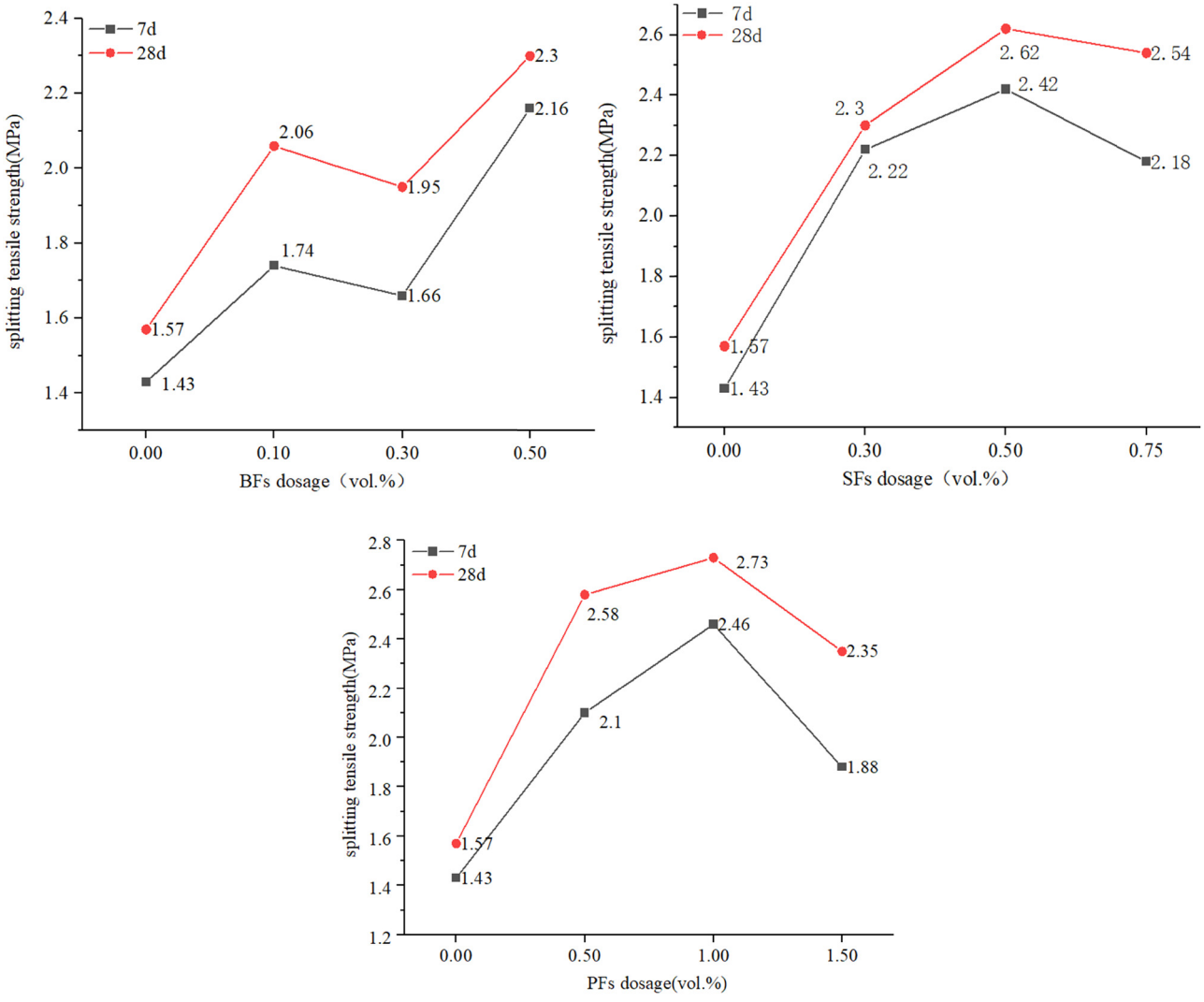

Figure 12: Splitting tensile strength of FRCGGPC.

At the same time, under the same fiber dosage, the improvement effect of BF on the splitting tensile strength of FRCGGPC is less than that of PF and SF. Comparing Figure 11, it can be seen that the 7 days splitting tensile strength of BFCGGPC was generally lower than that of PF and SF. After curing for 28 days, although the splitting tensile strength of control groups containing BF increased significantly, it was still inferior to PF and SF. The reasons are as follows: First, BF is mainly composed of SiO_2, Al_2O_3, CaO, and other compounds, which can react with strong alkaline solution and generate new aluminosilicate. Although the compressive strength of the matrix is improved, a part of BF will be dissolved in the process. When the dosage is not high, the number of fibers in the matrix that can bear the stress is less, and the limiting effect on crack generation and expansion is also weakened. Second, Some research results show that on the basis of this experiment, slightly increasing the dosage of BF can achieve better results. For example, the fiber-reinforced and toughened slag-coal FA-steel slag-based polymer cementitious material prepared by Xu *et al.* [47]. When the amount of basalt doping is increased to 0.6%, the mechanical properties of the specimens obtained are good, including the flexural strength reaching 10.8 MPa. Saloni *et al.* showed that BF exhibited positive effects on the fiber-matrix transition zone when the initial setting time, final setting time, bulk density, and compressive and flexural strengths were increased with the increased BF contents [48]. It can be seen that the optimal dosage range of BF in FRCGGPC can be further explored to optimize its mechanical properties.

3.2.3 Micromorphology analysis

Figures 13 and 15, respectively, show the 28 days microscopic morphology of the control groups BFCGGPC-0.5 group, SFCGGPC-0.5 group, and PFCGGPC-1.0 group under the splitting tensile test.

It can be seen from Figures 13–15 that there were no excessive dispersion between the phases of FRCGGPC, and the integrity was good. Each fiber was wrapped in the slurry. The interaction between the matrix and the fiber was obvious, and some fibers were pulled out. The above situation shows that the fibers share part of the external load and thus fracture, which shows that the fibers significantly increase the tensile strength of CGGPC.

According to the results of the splitting tensile test in this study, the three kinds of fibers had inconsistent improvement in the splitting tensile performance of CGGPC. Among them, SF has the best effect, followed by PF, and BF has the lowest enhancement. The reasons are analyzed from the micromorphology level as follows. As shown in Figure 13, first, BF was not wrapped in the matrix part of the smooth surface, with less adherent matrix and no obvious scratches,

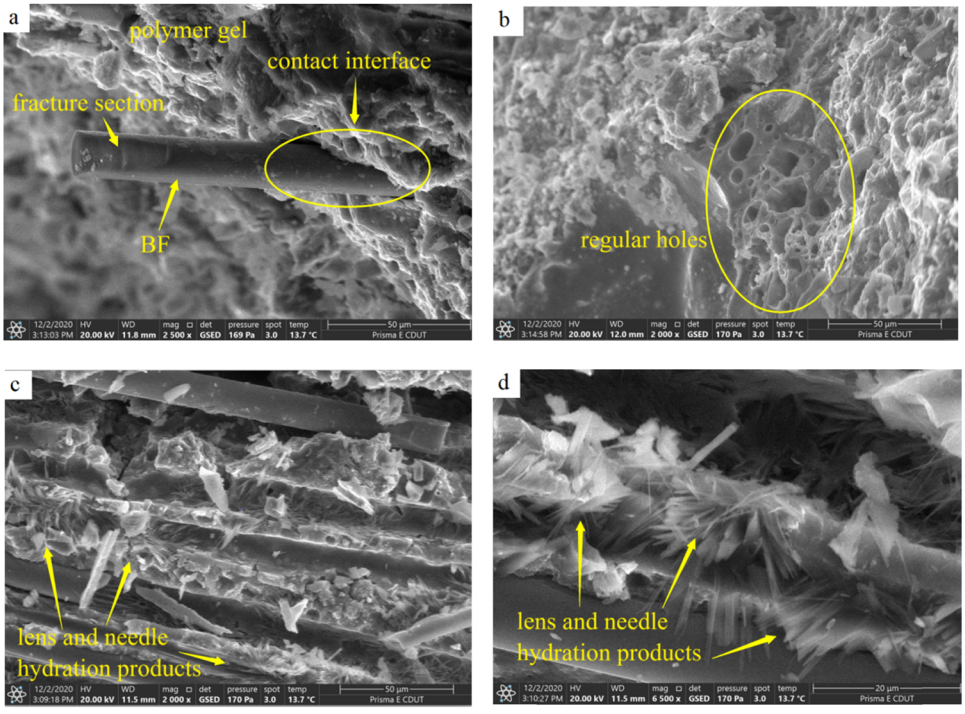

Figure 13: BFCGGPC-0.5. (a) mag2500× BF contact interface (b) mag2000× regular holes (c) mag2000× lens and needle hydration products (d) mag6500× lens and needle hydration products.

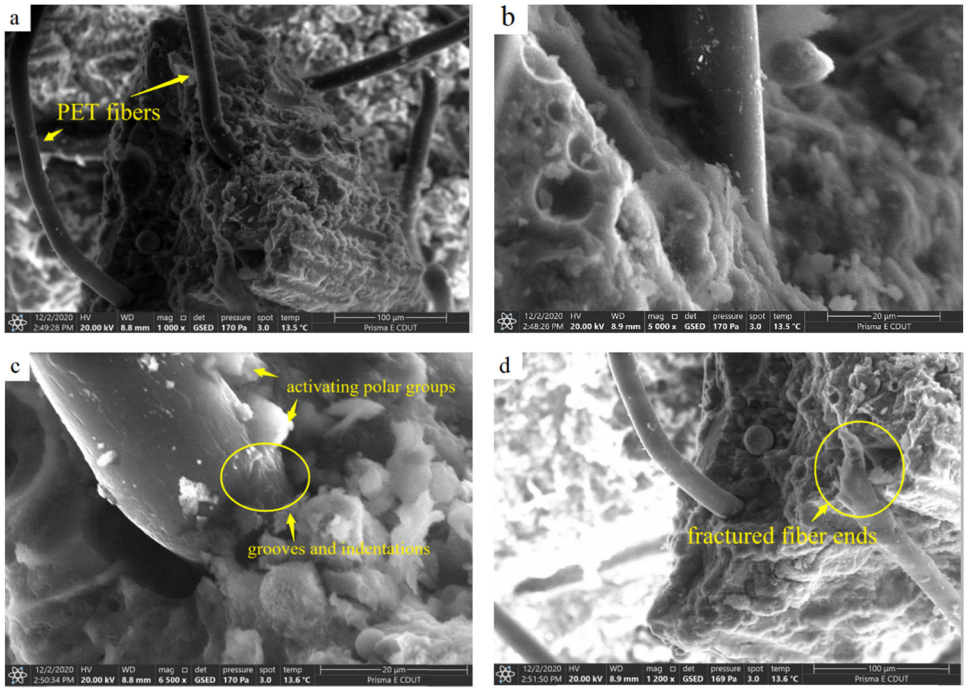

Figure 14: PFCGGPC-1.0. (a) mag1000× PET fibers (b) mag5000× PET fibers (c) mag6500× groups and grooves and indentations (d) mag1200× fractured fiber ends.

revealing a small gap between the root of the fiber and the contact part of the matrix. The fracture section of the fiber end was smooth, without tearing characteristics, which was brittle fracture. Second, it was clear that a large number of crystals and needle-shaped hydration products were attached around the BF, and some fibers' structure were incomplete. Therefore, this study believes that fibers are corroded in alkaline environment, and there is a phenomenon of reorganization after dissolution. This directly leads to a significant reduction in the number of fibers that can share the external load, and further weakens the limitation effect on the generation and expansion of cracks. In addition, the part of BF that can withstand the stress when subjected to damage does not have ductile characteristics. The surface was smooth, and the friction force between the BF and the matrix was relatively small.

However, the microscopic characteristics of PF and SF in the matrix were very different from those of BF. First of all, as shown in Figure 14, part of the surface of PF not wrapped in the matrix was not as smooth as BF. Some fiber surfaces not only had a small amount of adhesion matrix, but also had depressions and scratches, indicating that

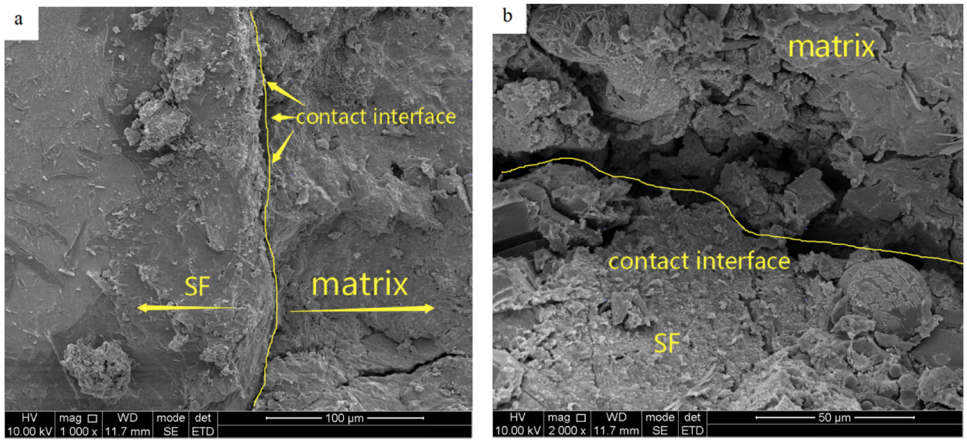

Figure 15: SFCGGPC-0.5. (a) mag1000× SF and matrix contact interface (b) mag2000× SF and matrix contact interface.

there was a certain friction between the fiber and the matrix. Ranjbar described the effect of fiber roughness on the local stress of the matrix [49]. The stress generated by the rough fiber at the contact interface is more complex, and the relative motion constraint on the fiber-matrix is stronger. The effect also radiates to the circular area at a certain distance from the contact interface. In addition, the smooth fiber will produce relative slip at the contact interface and the relative force is weaker. Second, PF is a kind of hydrophobic fiber, whose surface roughness is low. It can be improved by some surface treatment (such as fibrosis, indentation, and placement in alkaline environment) to strengthen the contact stress with the concrete matrix. The PFs in this experiment were roughened due to the dry alkaline environment. The adhesion matrix in Figure 14(c) was the activated polar group generated in the alkaline environment. In the process of mixing, the agglomeration phenomenon is obvious, and the dispersed fiber cannot give full play to the overall constraint effect on the matrix. At the same time, the agglomeration also leads to the formation of some holes in the matrix and the formation of weak links around it. Third, from Figure 14(d), it can be clearly seen that the end of a PF that was pulled off showed obvious tearing characteristics when it broke, and has a certain degree of deformation. This was the performance of its ductile characteristics, indicating that the PF was bridging the substrate while offsetting some of the energy from external loading. Eventually, it was pulled off when it reached its own ultimate bearing capacity.

The most significant effect of SFs on the splitting tensile performance of CGGPC is analyzed from the following two reasons. In the first place, as shown in Figure 15, the surface of SF is very rough, and it is wrapped with a large number of adhesion matrix. There is a strong contact stress (adhesion and friction) between the fiber and the matrix, which effectively restricts the relative motion of the fiber and the matrix and inhibits the generation of cracks. In the next place, the wavy structure of the SF itself substantially strengthens the mechanical bite between it and the matrix. In addition, the material characteristics that are not easy to break under the tensile condition of the SF make it fully play the bridging role in the whole loading process.

4 Conclusion

In this article, mechanical tests and micromorphology analysis of CGGPC with different fibers and dosages are carried out. The objectivity of mechanical properties test results is verified by micromorphology analysis. The main conclusions are as follows:

1) A certain dosage of BF, SF, and PF can slightly increase the compressive strength of CGGPC. The compressive strength of the control group containing BF continues to increase with the increase in the dosage, and its optimal dosage value can be further explored; The control group containing SF and PF has peak dosage. When the dosage is too high, the compressive strength will be lower than that of the benchmark group, showing a certain negative effect.
2) BF, SF, and PF have a significant effect on improving the splitting tensile strength of CGGPC. The improvement rate of 7 days splitting tensile strength of different control groups is about 16–72%, and the improvement rate of 28 days splitting tensile strength is about 44–73%. At the same dosage, the splitting tensile strength of SF- and PF- reinforced CGGPC is better than that of BF.
3) Within a certain dosage range, the three kinds of fibers are tightly wrapped in the matrix, and play a role in bearing part of the stress of the matrix. Under the compressive test, there is no obvious hole or loose matrix around the BF. The connection between the exposed fiber ends and the matrix is relatively tight, so the doping does not have adverse effects on the benchmark group's matrix; The gap between the SF and the matrix is wider, and the looseness near the matrix is also higher; PFs are interwoven with each other, causing agglomeration.
4) Under the splitting tensile test, the surface of BF is smooth, and there are voids at the root of contact with the matrix and dissolution occurring at some positions. The interaction force between this fiber and the matrix is weaker, and the number of fibers that can bear the tensile stress is small; While the surface of SF and PF is relatively rough, both have scratches and adherent matrix, and the adhesion performance of the interface between the fiber and matrix is good. The end of PF shows a tearing state with certain ductility characteristics. The unique wavy structure and performance characteristics of SF play a bridging role in the whole process of matrix cracking, which can effectively inhibit crack expansion and improve the macro mechanical properties of FRCGGPC.

This article compares the effect of three different FRCGGPCs on the mechanical properties and analyzes the microscopic mechanism, which provides a reference value for its research and application in the concrete industry. However, it can be seen from the test results and conclusions that there are still many problems

restricting the application and promotion of the material, such as small increase in strength at the later stage of curing and insufficient optimization of fiber types and additives. Subsequent studies hope to try compound addition of nanomaterials to explore the improvement and enhancement of the mechanical properties and durability performance of FRCGGPC, and further explore the internal mechanism and law of strength growth.

Acknowledgments: The writing of this article has been supported by many projects, which can be seen in funding information. At the same time, the project team members and all authors have supported this article. A note of thanks to them.

Funding information: This study was supported by Sichuan Mingyang Construction Engineering Management Co., Ltd. Specialized Project (MY2021-001), the Philosophy and Social Science Research Fund Project of Chengdu University of Technology (YJ2021-ZD002), Special Project of Marxist Theory Research of Chengdu University of Technology (20800-2021MLL005), Project of Western Ecological Civilization Research Center (XBST2021-YB002), Chengdu University of Technology Development Funding Program for Young and Middle-aged Key Teachers (10912-JXGG2021-01003), and College Students' Innovation and Entrepreneurship Training Program (202010616009, S202110616011, S2021106160114, S202110616013, and S202110616099).

Author contributions: All authors have accepted responsibility for the entire content of this manuscript and approved its submission.

Conflict of interest: The authors state no conflict of interest.

References

[1] Davidovits J. The ancient egyptian pyramids-concrete or rock. Concr Int. 1987;9(12):28–39.
[2] Davidovits J. Geopolymers and geopolymeric new materials. J Therm Anal Calorim. 1989;35(2):429–41.
[3] Davidovits J. Geopolymers: inorganic polymeric new materials. J Therm Anal Calorim. 1991;37(8):1633–56.
[4] Kurtoglu AE, Alzeebaree R, Aljumaili O, Nis A, Gulsan ME, Humur G, et al. Mechanical and durability properties of fly ash and slag based geopolymer concrete. Adv Concr Constr. 2018;6(4):345–62.
[5] Luhar S, Chaudhary S, Luhar I. Development of rubberized geopolymer concrete: strength and durability studies. Constr Build Mater. 2019;204:740–53.
[6] Xu Z, Huang ZP, Liu CJ, Deng XW, Hui D, Deng SJ, et al. Research progress on mechanical properties of geopolymer recycled aggregate concrete. Rev Adv Mater Sci. 2021;60(1):158–72.
[7] Ribeiro RAS, Ribeiro MGS, Sankar K, Kriven WM. Geopolymer-bamboo composite – a novel sustainable construction material. Constr Build Mater. 2016;123:501–7.
[8] Noushini A, Castel A. The effect of heat-curing on transport properties of low-calcium fly ash-based geopolymer concrete. Constr Build Mater. 2016;112:464–77.
[9] Liu CJ, Huang XC, Wu YY, Deng XW, Liu J, Zheng ZL, et al. Review on the research progress of cement-based and geopolymer materials modified by graphene and graphene oxide. Nanotechnol Rev. 2020;9(1):155–69.
[10] Amran YHM, Alyousef R, Alabduljabbar H, El-zeadani M. Clean production and properties of geopolymer concrete: a review. J Clean Prod. 2020;251:119679.
[11] Jiang X, Xiao R, Zhang MM, Hu W, Bai Y, Huang BS. A laboratory investigation of steel to fly ash-based geopolymer paste bonding behavior after exposure to elevated temperatures. Constr Build Mater. 2020;254:119267.
[12] Aguirre-guerrero AM, Robayo-salazar RA, de Gutierrez RM. A novel geopolymer application: coatings to protect reinforced concrete against corrosion. Appl Clay Sci. 2017;135:437–46.
[13] Xu Z, Huang ZP, Liu CJ, Deng XW, Hui D, Deng YT, et al. Experimental study on mechanical properties and microstructures of steel fiber-reinforced fly ash metakaolin geopolymer-recycled concrete. Rev Adv Mater Sci. 2021;60(1):578–90.
[14] Xu Z, Huang ZP, Liu CJ, Deng H, Deng XW, Hui D, et al. Research progress on key problems of nanomaterials-modified geopolymer concrete. Nanotechnol Rev. 2021;10(1):779–92.
[15] Zhang HY, Kodur V, Wu B, Yan J, Yuan ZS. Effect of temperature on bond characteristics of geopolymer concrete. Constr Build Mater. 2018;163:277–85.
[16] Gunasekara C, Setunge S, Law DW, Willis N, Burt T. Engineering properties of geopolymer aggregate concrete. J Mater Civ Eng. 2018;30(11):04018299.
[17] Biondi L, Perry M, Vlachakis C, Wu Z, Hamilton A, McAlorum J. Ambient-cured fly ash geopolymer coatings for concrete. Materials. 2019;12(6):923.
[18] Mendes SES, Oliveira RLN, Cremonez C, Pereira E, Trentin PO, Medeiros RA, et al. Estimation of electrical resistivity of concrete with blast-furnace slag. Aci Mater J. 2021;118(4):27–37.
[19] Mayhoub OA, Nasr EAR, Ali Y, Kohail M. Properties of slag based geopolymer reactive powder concrete. Ain Shams Eng J. 2021;12(1):99–105.
[20] Laskar SM, Talukdar S. Preparation and tests for workability, compressive and bond strength of ultra-fine slag based geopolymer as concrete repairing agent. Constr Build Mater. 2017;154:176–90.
[21] Alanazi H, Yang MJ, Zhang DL, Gao ZL. Bond strength of PCC pavement repairs using metakaolin-based geopolymer mortar. Cem Concr Comp. 2016;65:75–82.
[22] Alanazi H, Zhang DL, Yang MJ, Gao ZL. Early strength and durability of metakaolin-based geopolymer concrete. Mag Concr Res. 2017;69(1):46–54.
[23] Zhang DM, Ren FY. Study on coal gangue based geopolymer characteristics with dry powder activator. Non-Metallic Mines. 2016;39(6):35–7.

[24] Zhang WQ, Dong CW, Huang P, Sun Q, Li M, Chai J. Experimental study on the characteristics of activated coal gangue and coal gangue-based geopolymer. Energies. 2020;13(10):2504.
[25] Liu CJ, Deng XW, Liu J, Hui D. Mechanical properties and microstructures of hypergolic and calcined coal gangue based geopolymer recycled concrete. Constr Build Mater. 2019;221:691–708.
[26] Geng JJ, Zhou M, Li YX, Chen YC, Han Y, Wan S, et al. Comparison of red mud and coal gangue blended geopolymers synthesized through thermal activation and mechanical grinding preactivation. Constr Build Mater. 2017;153:185–92.
[27] Huang GD, Ji YS, Li J, Hou ZH, Dong ZC. Improving strength of calcinated coal gangue geopolymer mortars via increasing calcium content. Constr Build Mater. 2018;166:760–8.
[28] Liu CJ, Su X, Wu YY, Zheng ZL, Yang B, Luo YB, et al. Effect of nano-silica as cementitious materials-reducing admixtures on the workability, mechanical properties and durability of concrete. Nanotechnol Rev. 2021;10(1):1395–409.
[29] Liu CJ, Chen FL, Wu YY, Zheng ZL, Yang JW, Yang B, et al. Research progress on individual effect of graphene oxide in cement-based materials and its synergistic effect with other nanomaterials. Nanotechnol Rev. 2021;10(1):1208–35.
[30] Liu CJ, Huang XC, Wu YY, Deng XW, Zheng ZL. The effect of graphene oxide on the mechanical properties, impermeability and corrosion resistance of cement mortar containing mineral admixtures. Constr Build Mater. 2021;288:123059.
[31] Liu CJ, Huang XC, Wu YY, Deng XW, Zheng ZL, Xu Z, et al. Advance on the dispersion treatment of graphene oxide and the graphene oxide modified cement-based materials. Nanotechnol Rev. 2021;10(1):34–49.
[32] Liu CJ, He X, Deng XW, Wu YY, Zheng ZL, Liu J, et al. Application of nanomaterials in ultra-high performance concrete: a review. Nanotechnol Rev. 2020;9(1):1427–44.
[33] Saranya P, Nagarajan P, Shashikala AP. Performance studies on steel fiber- reinforced GGBS-dolomite geopolymer concrete. J Mater Civ Eng. 2021;33(2):04020447.
[34] Sahin F, Uysal M, Canpolat O, Aygormez Y, Cosgun T, Dehghanpour H. Effect of basalt fiber on metakaolin-based geopolymer mortars containing rilem, basalt and recycled waste concrete aggregates. Constr Build Mater. 2021;301:124113.
[35] Gao C, Huang L, Yan LB, Jin RY, Kasal B. Strength and ductility improvement of recycled aggregate concrete by polyester FRP-PVC tube confinement. Compos Part B-Eng. 2019;162:178–97.
[36] Zhou M, Xu M, Li ZW, Sun QW. Preparation and basic properties of spontaneous combustion gangue-slag-fly ash gepolyer. Bull Chin Ceram Soc. 2013;32(9):1826–31.
[37] Wang YC, Zhao JP, Tong YY, Ding JX. Different fiber toughened slag/fly ash based geopolymer. Bull Chin Ceram Soc. 2016;35(12):4173–9.
[38] Bhutta A, Borges PHR, Zanotti C, Farooq M, Banthia N. Flexural behavior of geopolymer composites reinforced with steel and polypropylene macro fibers. Cem Concr Comp. 2017;80:31–40.
[39] Shaikh FUA. Tensile and flexural behaviour of recycled polyethylene terephthalate (PET) fibre reinforced geopolymer composites. Constr Build Mater. 2020;245:118438.
[40] Bashar II, Alengaram UJ, Jumaat MZ, Islam A, Santhi H, Sharmin A. Engineering properties and fracture behaviour of high volume palm oil fuel ash based fibre reinforced geopolymer concrete. Constr Build Mater. 2016;111:286–97.
[41] Moradikhou AB, Esparham A, Avanaki MJ. Physical & mechanical properties of fiber reinforced metakaolin-based geopolymer concrete. Constr Build Mater. 2020;251:118965.
[42] Liu YW, Shi CJ, Zhang ZH, Li N, Shi D. Mechanical and fracture properties of ultra-high performance geopolymer concrete: effects of steel fiber and silica fume. Cem Concr Comp. 2020;112:103665.
[43] Liu YW, Zhang ZH, Shi CJ, Zhu DJ, Li N, Deng YL. Development of ultra-high performance geopolymer concrete (UHPGC): influence of steel fiber on mechanical properties. Cem Concr Comp. 2020;112:103670.
[44] Yang MQ, Li WG, He Y, Zhang XY, Li Y, Zhao ZY, et al. Modeling the temperature dependent ultimate tensile strength of fiber/polymer composites considering fiber agglomeration. Compos Sci Technol. 2021;213:108905.
[45] Tang C, Li X, Tang YJ, Zeng J, Xie JY, Xiong BF. Agglomeration mechanism and restraint measures of SiO_2 nanoparticles in meta-aramid fibers doping modification via molecular dynamics simulations. Nanotechnology. 2020;31(16):165702.
[46] Punurai W, Kroehong W, Saptamongkol A, Chindaprasirt P. Mechanical properties, microstructure and drying shrinkage of hybrid fly ash-basalt fiber geopolymer paste. Constr Build Mater. 2018;186:62–70.
[47] Xu Y, Zhang YJ, Wang YC, Xu DL. Preparation of ternary geopolymer toughened by basalt fiber. N Chem Mater. 2011;39(11):128–31.
[48] Saloni, Parveen, Pham TM. Enhanced properties of high-silica rice husk ash-based geopolymer paste by incorporating basalt fibers. Constr Build Mater. 2020;245:118422.
[49] Ranjbar N, Zhang MZ. Fiber-reinforced geopolymer composites: a review. Cem Concr Comp. 2020;107:103498.